Convergent EKF-based control allocation: general formulation and application to a Control Moment Gyro cluster

Ervan Kassarian, Mathieu Rognant, Helene Evain, Daniel Alazard, Corentin Chauffaut

2020 American Control Conference
Denver, CO, USA, July 1-3, 2020

Convergent EKF-based control allocation: general formulation and application to a Control Moment Gyro cluster.

Ervan Kassarian[1], Mathieu Rognant[2], Helene Evain[3], Daniel Alazard[1], Corentin Chauffaut[1]

***Abstract*— This paper addresses control allocation for redundant systems with the Extended Kalman Filter formalism. This method is compatible with the low computational power available in space environment, and presents a flexible framework to include constraints such as singularity avoidance. The convergence domain of the allocator is derived from the contraction theory framework, depending on specific parameters of the system. A general formulation is proposed to maximize the convergence domain with regard to these parameters. The method is applied to design a steering law of Control Moment Gyroscopes. Experimental tests show that the control allocation allows the actuators to work efficiently along nominal trajectories while avoiding singularities when necessary.**

Keywords: control allocation, redundant actuators, Extended Kalman Filter, singularity, Control Moment Gyro

I. INTRODUCTION

The control architecture of an over-actuated system usually consists of three levels [1] as shown in Fig.1. First, a high level controller computes the control efforts that are needed to perform the desired overall motion. Next, control allocation coordinates the set of actuators to generate the required forces or torques on the system. Last, low-level control algorithms ensure that each individual actuator follows a desired closed-loop dynamic.

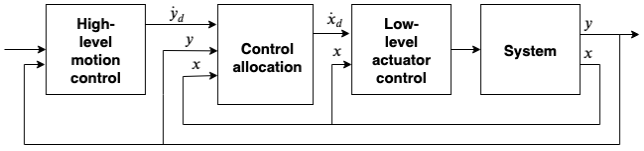

Fig. 1: A common control architecture for redundant systems

As presented in [1], the three levels of command can be handled with a modular approach. While the high-level controller usually adjusts the performances of the closed-loop system, control allocation addresses specific constraints such as saturation or power efficiency. Moreover, so-called singular configurations exist for which the actuators locally become unable to work in a given direction. Control allocation must address these singularities as well.

This paper focuses on the control allocation and its real-time implementation in robotics system. For a wide range of mechanical systems such as multi-degree-of-freedom manipulator arms, cable robots, submarines or satellites, the dynamic model is linear in the control input:

$$\begin{cases} \dot{\mathbf{x}} = \mathbf{f}(\mathbf{x}) + \mathbf{G}(\mathbf{x})\mathbf{u} \\ \mathbf{y} = \mathbf{h}(\mathbf{x}) \end{cases} \tag{1}$$

with $\mathbf{x} \in \mathbb{R}^n$ the state, $\mathbf{u} \in \mathbb{R}^l$ the control input, $\mathbf{y} \in \mathbb{R}^m$ the controlled output with $l > m$, $\mathbf{G} \in \mathbb{R}^{n \times l}$, $\mathbf{f}$ and $\mathbf{h}$ differentiable functions (in this paper, vectors are written in bold small letters and the matrices are in bold capital letters).

Then, as proposed in [2], the allocation problem can be rewritten under the classic form addressed in [3]:

$$\dot{\mathbf{y}} = \mathbf{J}(\mathbf{x})\dot{\mathbf{x}} \tag{2}$$

where $\mathbf{J}(\mathbf{x}) = \frac{\partial \mathbf{h}}{\partial \mathbf{x}}$ is the Jacobian matrix of the non-linear function $\mathbf{h}$ depending on the configuration $\mathbf{x}$.

Numerous allocation methods are proposed in the literature to perform the nonlinear dynamic inversion of (2), often based on the Moore-Penrose pseudo-inversion:

$$\dot{\mathbf{x}} = \mathbf{J}^T(\mathbf{J}\mathbf{J}^T)^{-1}\dot{\mathbf{y}} = \mathbf{J}^\dagger\dot{\mathbf{y}} \tag{3}$$

However, the matrix $\mathbf{J}^\dagger$ is undefined for singular configurations, that is, when $\mathbf{J}\mathbf{J}^T$ is not invertible, and a Moore-Penrose allocation leads to saturations of the system in the vicinity of such singularities. To ensure the invertibility of the system, [4] and [5] proposed the Singular Inverse Robust method (SRI) which consists in inverting $\mathbf{J}\mathbf{J}^T + \lambda\mathbf{I}$ instead of $\mathbf{J}\mathbf{J}^T$, with λ a tunable parameter. For example, [6] proposes to adjust λ dynamically using the singular values of $\mathbf{J}$ but this requires to perform a singular value decomposition. Adjustments with smaller computational costs exist but they may induce larger errors and slow convergence [7]. The additional degrees of freedom provided by a redundant system also motivate optimization-based solutions. For example, quadratic programming [8] or fixed-point method [9] are adequate to address the allocation problem. However, their iterative nature leads to high computational costs.

An allocation method using the Extended Kalman Filter (EKF) formalism was introduced in [2] as an interesting alternative to the existing allocation algorithms. This EKF-based allocator is compliant with real-time constraints while addressing the singularity avoidance and saturation management. It also provides flexibility regarding additional constraints that can be added as equations with the covariance matrices sizing their relative weights. Furthermore, the convergence of the allocator can be studied with the literature results concerning the stability of the EKF in general.

[1] ISAE, Toulouse, France. D. Alazard is an AIAA Associate Fellow.
[2] ONERA, Toulouse, France
[3] CNES, Toulouse, France
email: ervan.kassarian@isae-supaero.fr

In this paper, the recent development on the contraction framework [10] is investigated to derive a general formulation of convergent EKF-based allocators. In a first part, convergence proofs are briefly reminded to highlight the main parameters that should be considered to ensure a suitable convergence domain of the allocator. Then, in a second part, a general formulation of a discrete EKF-based allocator is presented. The proposed formulation aims at maximizing the convergence domain while handling the system specifications and the allocator implementation. Finally, in a third part, this method is applied to a cluster of Control Moment Gyroscopes (CMGs) and tests are carried out. Contributions regarding the previous work [2] are essentially the new convergence proof based on the contraction framework and the experimental validation.

II. Convergence analysis

It is essential to ensure the convergence of the allocation control toward an optimal solution. Proofs already exist for allocation methods but most of them are closed-loop results [11], [12]. The convergence of the EKF-based allocator has the advantage that standard EKF stability results are applicable, as stated in [2]. Thus convergence of the control allocation can be assessed whatever the high-level motion controller used (Fig.1).

The convergence proof as originally used in [2] relies on a Lyapunov approach [13]. The recent work on the contraction framework exploits a different approach of the notion of stability, as described in [14]. While the Lyapunov framework directly studies the evolution of the discrepancy between the estimated state and the true state, the contraction theory analyses whether nearby trajectories converge to one another. As a consequence, the convergence criterion derived in [10] is generally less conservative and is used in this paper.

A. Assumptions

Consider the estimation model:

$$\widehat{\mathbf{v}}_k = \mathbf{f}_k(\mathbf{v}_{k-1}) + \boldsymbol{\varepsilon}_v, \quad \mathbf{m}_k = \mathbf{g}_k(\widehat{\mathbf{v}}_k) + \boldsymbol{\varepsilon}_m \tag{4}$$

with $\mathbf{v}_k$ the state estimate vector at step k, $\widehat{\mathbf{v}}_k$ the predicted state vector, $\mathbf{m}_k$ the measurement vector, $\boldsymbol{\varepsilon}_v$ (resp. $\boldsymbol{\varepsilon}_m$) the prediction (resp. measurement) error characterized by the covariance matrices $\mathbf{Q}_k$ (resp. $\mathbf{R}_k$). Let us note $\mathbf{P}_k$ the covariance of the estimation error, $\mathbf{F}_k$ (resp. $\mathbf{C}_k$) the Jacobian matrix of $\mathbf{f}_k$ (resp. $\mathbf{g}_k$), and $\mathbf{D^2 f}_k$ (resp. $\mathbf{D^2 g}_k$) the corresponding Hessian tensor.

Assuming that each of the EKF matrices is positive definite and bounded, let us define for any step k the following bounds with the 2-norm:

$$\begin{aligned} \underline{f}\mathbf{I} \leq \mathbf{F}_k \leq \bar{f}\mathbf{I}, \quad \underline{c}\mathbf{I} \leq \mathbf{C}_k \leq \bar{c}\mathbf{I} \\ \underline{q}\mathbf{I} \leq \mathbf{Q}_k \leq \bar{q}\mathbf{I}, \quad \underline{r}\mathbf{I} \leq \mathbf{R}_k \leq \bar{r}\mathbf{I} \end{aligned} \tag{5}$$

Under these assumptions, $\mathbf{P}$ can be bounded, which is necessary to apply the results of [10]. Furthermore, it is assumed that the prediction is linear and the Hessian $\mathbf{D^2 g}_k$ is bounded:

$$|||\, \mathbf{D^2 f}_k \,||| = 0, \quad |||\, \mathbf{D^2 g}_k \,||| \leq \kappa_C \tag{6}$$

The latter assumption is sufficient to derive the convergence domain proposed in [10].

B. Bounding the covariance P

Let us write the EKF equations for the state covariance P under their information form as in [15]:

$$\mathbf{P}_{k+1|k} = \mathbf{F}_k \mathbf{P}_k \mathbf{F}_k^T + \mathbf{Q} \tag{7}$$

$$\mathbf{P}_{k+1}^{-1} = \mathbf{P}_{k+1|k}^{-1} + \mathbf{C}_k^T \mathbf{R}_k^{-1} \mathbf{C}_k \tag{8}$$

Assuming that $\mathbf{P}$ is already bounded at a given step k, and under assumption (5), then $\mathbf{P}$ is bounded at step $k+1$:

$$\underline{p}I \leq \mathbf{P}_k \leq \bar{p}I \Rightarrow \underbrace{\frac{1}{\frac{1}{\underline{f}^2 \underline{p} + \underline{q}} + \frac{\underline{c}^2}{\underline{r}}}}_{\underline{p}^+(\underline{p})} \mathbf{I} \leq \mathbf{P}_{k+1} \leq \underbrace{\frac{1}{\frac{1}{\bar{f}^2 \bar{p} + \bar{q}} + \frac{\underline{c}^2}{\bar{r}}}}_{\bar{p}^+(\bar{p})} \mathbf{I} \tag{9}$$

By induction, solving $\underline{p}_0 = \underline{p}^+(\underline{p}_0)$ and $\bar{p}_0 = \bar{p}^+(\bar{p}_0)$ provides bounds $\underline{p}_0$ and $\bar{p}_0$ for $\mathbf{P}_0$ that will hold for any $k \geq 0$.

C. Domain of convergence

Under the aforementioned assumptions, [10] guarantees the convergence of the EKF for an initial error inferior to:

$$||\, \mathbf{e}_0 \,|| \leq \sqrt{\frac{\underline{p}}{\bar{p}}} \frac{\sqrt{\underline{q}\underline{r}}}{\sqrt{2}\kappa_C \bar{p}} \tag{10}$$

An adequate set of matrices bounds is essential to yield non-conservative bounds of $\mathbf{P}$ in (9) and strong convergence guarantee in (10).

The bounds of the Jacobian matrices $\mathbf{F}$ and $\mathbf{C}$ and covariance matrices $\mathbf{Q}$ and $\mathbf{R}$ essentially derive from the choice of the state vector as well as the prediction and measurement equations. For the implementation in a given system, the dynamic (2) has to be discretized and linearized. The risk of divergence of the control allocation arises from this linearization. In the current work, the linearization error is taken into account with the bound κ_C of the Hessian $\mathbf{D^2 g}_k$. The proposed formulation takes advantage of the explicit expression of the convergence domain (10) to ensure its compliance with the system specifications.

To conclude the convergence analysis, the contraction theory provides a general framework to characterize the stability of the EKF. Under a few assumptions, a general expression of the convergence domain can be obtained. The influence of the system specifications on this expression can be explicitly derived within the proposed EKF formulation to maximize the convergence of the allocation control.

III. A general formulation of the EKF-based allocator

In this part, a general formulation of an EKF-based allocator is proposed to perform the dynamic inversion of (2) while verifying assumptions (5) and (6) and optimizing the guaranteed convergence domain (10) with regard to the system specific features.

Similarly to a Recursive Least-Squares approach [16], the EKF minimizes the following criterion:

$$\min_{\mathbf{v}} \left\{ (\mathbf{m}-\mathbf{g}(\widehat{\mathbf{v}}))^T \mathbf{R}^{-1} (\mathbf{m}-\mathbf{g}(\widehat{\mathbf{v}})) + (\widehat{\mathbf{v}}-\mathbf{v}) \mathbf{P}^{-1} (\widehat{\mathbf{v}}-\mathbf{v}) \right\} \tag{11}$$

Regarding (11), the proposed method is close to optimization-based allocators such as in [8], yet requires lower computational load due to its recursive nature. With this in mind, the EKF equations can be seen as deterministic constraints, and the covariance matrices as weights associated to these constraints. In the following sections, we propose to define the weight of each equation accordingly to the specifications of the considered system. One weight will depend on the current state of the system in order to allow singularity avoidance. The other weights will be constant and essentially aim at limiting the actuators' efforts with regard to their maximum capacities.

A. Normalized state variables

It is assumed that, when the control allocation function is called at a given time t, the vectors $\mathbf{x}(t)$ and $\dot{\mathbf{x}}(t)$ are measured and provided to the EKF. As presented in Fig.1, allocation control computes the desired command $\dot{\mathbf{x}}_d(t+T_s)$ to be sent to the actuators, where t is the current time and T_s is the sampling time of the allocator.

Let $\dot{x}_n$ and $\dot{y}_n$ be two normalization parameters that can be adjusted to ensure a proper conditioning of the matrices, and let us define the state vector as:

$$\mathbf{v} = \begin{bmatrix} \mathbf{v}_1 \\ \mathbf{v}_2 \end{bmatrix} = \begin{bmatrix} \frac{\dot{\mathbf{x}}_d(t+T_s)}{\dot{x}_n} \\ \frac{\dot{\mathbf{y}}(t+T_s)}{\dot{y}_n} \end{bmatrix} \in \mathbb{R}^{m+n} \tag{12}$$

B. Prediction phase

This phase consists in predicting the same solution as in previous step:

$$\begin{aligned} \widehat{\mathbf{v}}_1(t+T_s) &= \mathbf{v}_1(t) + \boldsymbol{\varepsilon}_{v1} \\ \widehat{\mathbf{v}}_2(t+T_s) &= \mathbf{v}_2(t) + \boldsymbol{\varepsilon}_{v2} \end{aligned} \tag{13}$$

Considering criterion (11), prediction phase formulates a constraint on the accelerations $\dot{\mathbf{x}}_d(t+T_s) - \dot{\mathbf{x}}(t)$ and $\dot{\mathbf{y}}(t+T_s) - \dot{\mathbf{y}}(t)$. More specifically, the prediction model weights solutions with constant rate. This helps limiting the actuators' effort and preventing saturation. Thus, the associated weights – the covariance of $\boldsymbol{\varepsilon}_{v1}$ and $\boldsymbol{\varepsilon}_{v2}$ – can be defined with regard to the maximum capacities of the system.

C. Correction phase

In this phase, the allocation dynamic (2) is formulated as a measurement equation. Two other measurement equations are formulated to produce the desired command $\dot{\mathbf{y}}_d$ while ensuring the avoidance of singularities and saturation.

The first measurement equation constrains the state variables to respect the dynamic (2):

$$\mathbf{0}_{n\times 1} = \mathbf{m}_1 = \frac{\mathbf{J}(\mathbf{x}(t+T_s))\,\dot{\mathbf{x}}(t+T_s) - \dot{\mathbf{y}}(t+T_s)}{\dot{y}_n} + \boldsymbol{\varepsilon}_{m1} \tag{14}$$

This equation is not linear. The associated covariance can be defined as an estimation of the maximum error $\Delta\dot{y}_{err}$ when linearizing the allocation problem (2).

The tracking of the reference $\dot{\mathbf{y}}_d$ is constrained by the second measurement equation:

$$\frac{\dot{\mathbf{y}}_d}{\dot{y}_n} = \mathbf{m}_2 = \mathbf{v}_2 + \boldsymbol{\varepsilon}_{m2} \tag{15}$$

Its covariance mainly depends on the distance to singularities, which can be evaluated with the scalar $det(\mathbf{J}\mathbf{J}^T)$ – it is a continuous function that equals 0 for singular configurations. Far from any singularity, the covariance value is set to a minimum so as to precisely generate the desired task. However, close to a singular configuration, the inversion of the dynamic (2) becomes an ill-conditioned problem. In this case, increasing the covariance loosens the constraint on the reference tracking. In combination with next measurement equation, this allows to avoid singularities.

The actuators constraint on $\dot{\mathbf{x}}$ is handled with the third measurement equation:

$$0 = \mathbf{m}_3 = \mathbf{v}_1 + \boldsymbol{\varepsilon}_{m3} \tag{16}$$

with a covariance sized with the maximum capacity in speed of the system. With respect to the criterion (11), this equation helps minimizing the actuators' effort – represented by a quadratic expression in $\dot{\mathbf{x}}_d(t+T_s)$ – such as proposed in [8] with a standard optimization approach. This is valuable not only for power efficiency, but also for singularity avoidance. Indeed, heading toward a singularity will require increasing efforts from the actuators to compensate for their loss of capacity in the singular direction. This is prevented by limiting the efforts of the actuators. In this formulation, singularity avoidance essentially arises from the optimal solution of (11) being balanced between the reference tracking (15) and the actuators restriction (16).

D. Evaluation and maximization of the convergence domain

The equations formulated above cover the resolution of the allocation problem with the EKF formalism. In this part, the evaluation of the convergence domain is addressed as well as its maximization using the normalization parameters of the state vector.

With the notations of II-A, $\mathbf{F}$ is the Jacobian matrix of the prediction equation (13) and $\mathbf{Q}$ is the related covariance:

$$\mathbf{F} = \mathbf{I}_{m+n}, \quad \mathbf{Q} = diag\left(\left(\frac{T_s \ddot{x}_{max}}{\dot{x}_n} \right)^2 \mathbf{I}_n,\ \left(\frac{T_s \ddot{y}_{max}}{\dot{y}_n} \right)^2 \mathbf{I}_m \right) \tag{17}$$

To derive the Jacobian matrix $\mathbf{C}$, it is first necessary to find $\frac{\partial \mathbf{g}_1}{\partial \dot{\mathbf{x}}_d}$ – corresponding to the first measurement equation (14). To do so, let us write the first order approximation of the dynamic equation (2) between t and $t+T_s$:

$$\Delta\dot{\mathbf{y}} \approx \frac{\partial \mathbf{J}(\mathbf{x})\dot{\mathbf{x}}}{\partial \mathbf{x}} \Delta\mathbf{x} + \mathbf{J}(\mathbf{x}) \Delta\dot{\mathbf{x}} \tag{18}$$

As shown in Fig.1, the actuators generating $\dot{\mathbf{x}}$ are generally controlled in a low-level closed-loop. This controller is

typically tuned to impose a first-order or a damped second-order dynamic. In this context, it can be assumed that:

$$\begin{aligned} \Delta\dot{\mathbf{x}} &= \alpha\left(\dot{\mathbf{x}}_d(t+T_s) - \dot{\mathbf{x}}(t)\right) \\ \Delta\mathbf{x} &= T_s\dot{\mathbf{x}}(t) + T_a\left(\dot{\mathbf{x}}_d(t+T_s) - \dot{\mathbf{x}}(t)\right) \end{aligned} \tag{19}$$

where α and T_a are parameters depending on the closed-loop dynamic of the actuators and of the sampling time T_s.

From (14), (15), (16), (18) and (19), the measurement matrix $\mathbf{C}$ can be written:

$$\mathbf{C} = \frac{\partial \mathbf{g}}{\partial \mathbf{v}} = \begin{bmatrix} \left(\alpha\mathbf{J}(\mathbf{x}) + T_a\frac{\partial \mathbf{J}(\mathbf{x})\dot{\mathbf{x}}}{\partial \mathbf{x}}\right)\frac{\dot{x}_n}{\dot{y}_n} & -\mathbf{I}_m \\ \mathbf{0}_{m\times n} & \mathbf{I}_m \\ \mathbf{I}_n & \mathbf{0}_{n\times m} \end{bmatrix} \tag{20}$$

And the associated diagonal covariance matrix:

$$\mathbf{R} = diag\left(\left(\frac{\Delta\dot{y}_{err}}{\dot{y}_n}\right)^2\mathbf{I}_m,\ r_2\mathbf{I}_m,\ \left(\frac{\dot{x}_{max}}{\dot{x}_n}\right)^2\mathbf{I}_n\right) \tag{21}$$

The bounds of $\mathbf{R}$ can be set by $\left(\frac{\Delta\dot{y}_{err}}{\dot{y}_n}\right)^2$ and $\left(\frac{\dot{x}_{max}}{\dot{x}_n}\right)^2$. Then, r_2 can be chosen as a decreasing function of $det(\mathbf{J}\mathbf{J}^T)$ as long as it stays between these bounds.

Similarly, the Hessian matrix derives from the second-order approximation of the dynamic equation (2) and its bound κ_C can be computed for the considered application. The proposed matrices verify assumptions (5) and (6). In particular, the Jacobian matrices keep full rank even when $\mathbf{J}(\mathbf{x})$ is rank deficient.

The bounds of the matrices, thus the convergence domain (10), are functions of the normalization parameters $\dot{x}_n$ and $\dot{y}_n$. For given values of $\dot{x}_n$ and $\dot{y}_n$, they can be numerically evaluated given the system specifications: $\dot{x}_{max}$, $\ddot{x}_{max}$, $\dot{y}_{max}$, $\ddot{y}_{max}$, $\Delta\dot{y}_{err}$, T_s, α, T_a, and matrices $\mathbf{J}(\mathbf{x})$ and derivatives of $\mathbf{J}(\mathbf{x})\dot{\mathbf{x}}$. The values of $\dot{x}_n$ and $\dot{y}_n$ must be chosen such that the convergence domain is greater than the maximum error $||\ \mathbf{e}_0\ ||$ on the state vector $\mathbf{v}$, that derives directly from the system specifications T_s, $\ddot{x}_{max}$, $\ddot{y}_{max}$ and from the parameters $\dot{x}_n$ and $\dot{y}_n$ according to the expression of $\mathbf{v}$ in (12). It is also important to ensure that the matrices' bounds do not fall below a threshold given by the numerical precision of the on-board computer.

These two conditions may not be simultaneously verified. In this case, two possible trade-offs arise regarding (10) to guarantee the convergence. Increasing $\underline{r}$, the lower bound of the measurement covariance, improves the convergence domain at the expense of the precision on the equations of the dynamic (14) and of the reference command tracking (15). Decreasing $||\ \mathbf{e}_0\ ||$ by decreasing $\ddot{x}_{max}$ and $\ddot{y}_{max}$ constrains the system capacities to ensure the numerical stability of the allocation control.

IV. Application to a Control Moment Gyro Cluster

In this section, the proposed procedure is applied to design a steering law of a six Control Moment Gyro (CMG) cluster in a pyramidal configuration. CMGs are used to perform satellite attitude control and operate by kinetic momentum transfer between the satellite frame and flywheels spinning at a constant rate. More efficient than reaction wheels, in particular with respect to their torque capabilities, the drawbacks of these actuators lie in the complexity of their steering law and mechanism. These points prevent their use in low-cost nano-satellites with short design times. To increase the technology readiness level of CMGs for the nano-satellites market, an experimental setup with six CMGs was designed and presented in [17]. This setup has been successfully tested in micro-gravity conditions [18] during a European Space Agency (ESA) parabolic flight campaign. First, the modelling and the main characteristics of this test bench are reminded. Next, the implementation of the allocator is detailed. Last, experimental results are presented.

A. Description of the experimental setup

A Control Moment Gyro is composed of a flywheel that spins at a constant rate, creating a fixed angular momentum along an axis $\boldsymbol{x}_i$. Rotating the axis of rotation of the flywheel along an axis $\boldsymbol{z}_i$, named gimbal axis, creates a gyroscopic torque on the $\boldsymbol{y}_i$ axis, as described in Fig 2a.

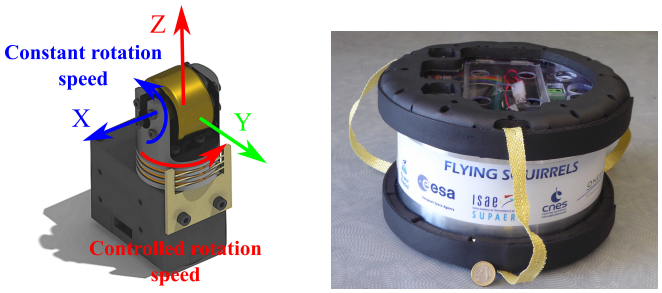

(a) CMG principle (b) Test bench

Fig. 2: Presentation of the experimental setup

The flywheels are actuated by small sensor-less brushless motors regulated at a constant speed thanks to back Electro Motive Force estimation. The gimbal axes are actuated by servo module actuators including controller, driver and network interfaces. These modules perform a speed control by using absolute rotary encoders. After identification, the closed loop dynamic of the gimbal axis could be approximated as a first order with a rising time of 200 ms. This control is robust to the gyroscopic torques induced by the angular velocity of the platform. The setup is autonomous in energy and is equipped with an inertial measurement unit and a monocular camera. The on-board computer is a Raspberry Pi 3 which performs the estimation of the platform state and computes the gimbal axis velocities references. These functionalities are implemented as distinct software components in a Robot Operating System (ROS) middleware. The test bench is shown in Fig.2b.

B. Application of the proposed method

The system is a cluster of $n = 6$ Control Moment Gyroscopes. The angular position of the i-th gyroscope around $\boldsymbol{z}_i$ is noted σ_i. Let $\boldsymbol{\sigma} \in \mathbb{R}^n$ be the vector composed of

the n angular positions. Let h_t be the norm of the kinetic momentum of a single flywheel (constant and identical for all of them), along $\boldsymbol{y}_i$. The torque created by the i-th gyroscope is:

$$\dot{\mathbf{h}}_i = h_t \dot{\sigma}_i \boldsymbol{y}_i \tag{22}$$

Let $\mathbf{Y}(\boldsymbol{\sigma})$ be the concatenation of the axes $\boldsymbol{y}_i$ in the satellite frame: $\mathbf{Y}(\boldsymbol{\sigma}) = [\boldsymbol{y}_1(\sigma_1) \ \ldots \ \boldsymbol{y}_n(\sigma_n)]$. The torque created by the CMG cluster is written:

$$\dot{\mathbf{h}} = h_t \mathbf{Y}(\boldsymbol{\sigma}) \dot{\boldsymbol{\sigma}} \tag{23}$$

Therefore, this control allocation problem can be addressed using the proposed method with $\mathbf{v}_1 = \frac{\dot{\boldsymbol{\sigma}}}{\dot{\sigma}_n}$ and $\mathbf{v}_2 = \frac{\dot{\mathbf{h}}}{\dot{h}_n}$. On the experimental test bench, the rotation speeds $\dot{\sigma}_i$ and the accelerations $\ddot{\sigma}_i$ cannot exceed $\pm 5 \ rad/s$ and $\pm 50 \ rad/s^2$ respectively. An analysis of the singular values of $\mathbf{Y}(\boldsymbol{\sigma})$ showed that the maximum capacity in torque was $\dot{\mathbf{h}}_{max} = 2.2 h_t \dot{\sigma}_{max}$. The refreshing rate of the allocation control is $\frac{1}{T_s} = 16 Hz$.

The bounds of the matrices were evaluated according to the matrix $\mathbf{Y}(\boldsymbol{\sigma})$ and the system parameters. With the values $\dot{\sigma}_n = 300 \ rad/s$ and $\dot{h}_n = 660 \ h_t$, the convergence domain was compliant with the maximum capacities in torque and actuators speeds while all the numerical bounds were kept above 10^{-7}.

C. Experimental results

The test bench is maintained motionless. The total angular momentum $\mathbf{h}$ created by the cluster of 6 CMGs is evaluated using the vector of angular positions $\boldsymbol{\sigma}$ and controlled in feedback with regard to a reference value $\mathbf{h}_d$ reached after a ramp of 2 s. The high-level controller is a single gain $k_p = \frac{1}{5T_s}$ computing the allocator's input torque $\dot{\mathbf{h}}_d$.

Two reference inputs $\mathbf{h}_d$ are tested. The first one is close to the maximum capacity of the CMGs cluster. The second one is chosen so that the trajectory meets a singularity. For the latter, the EKF-based allocation is compared with a classical Moore-Penrose inversion to illustrate the capacity of the method to avoid singularities.

1) Reference trajectory – without singularity: Fig.3 shows the experimental results for a desired angular momentum:

$$\mathbf{h}_d = \begin{bmatrix} 0 & 0 & 0.025 \end{bmatrix} N.m.s \tag{24}$$

Top-down are plotted the angular momentum $\mathbf{h}$ of the bench compared to the desired vector $\mathbf{h}_d$, the determinant $det(\mathbf{Y}\mathbf{Y}^T)$, the desired rotation speeds sent to the CMGs (the output of the allocator), and the projection of these rotation speeds onto the kernel space of $\mathbf{J}(\mathbf{x})$.

The determinant $det(\mathbf{Y}\mathbf{Y}^T)$ is a measure of the distance to singularities: it is a continuous function that equals 0 for singular configurations. Here it decreases after $5s$ because the configuration is approaching the maximum capacity of the cluster in angular momentum, which is an external singularity. However, there is no internal singularity along the trajectory and the reference tracking is satisfying.

The kernel space of $\mathbf{Y}(\boldsymbol{\sigma})$ regroups the rotation speeds $\dot{\boldsymbol{\sigma}}$ that do not produce any resulting torque : $\dot{\mathbf{h}} = \mathbf{Y}(\boldsymbol{\sigma}) \dot{\boldsymbol{\sigma}}_{ker} = \mathbf{0}$.

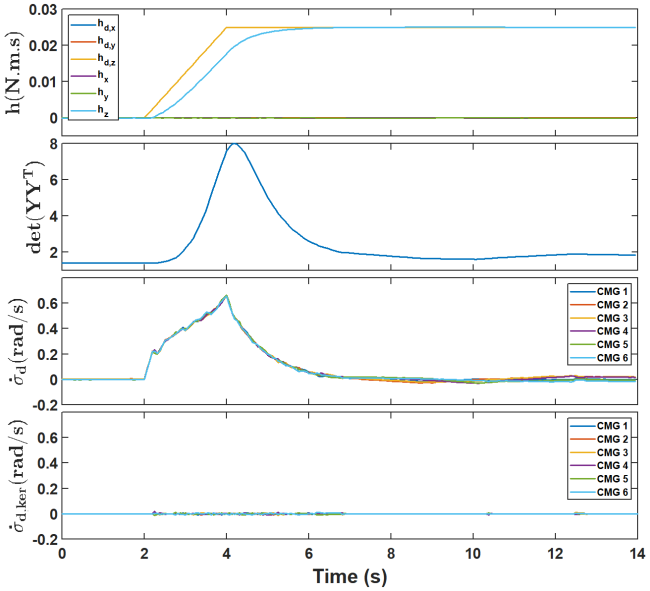

Fig. 3: Reference trajectory with the EKF control allocation

Hence, the projection of the rotation speeds $\dot{\boldsymbol{\sigma}}$ onto the kernel space of of $\mathbf{Y}(\boldsymbol{\sigma})$ represent efforts of the actuators that do not contribute to any output torque. In this case, the vector of the rotation speeds $\dot{\boldsymbol{\sigma}}$ stays orthogonal to the kernel space. This means that the efforts are minimized – accordingly to the third measurement equation (16).

2) Singularity avoidance: The following reference direction was chosen so as to meet a singular configuration:

$$\mathbf{h}_d = \begin{bmatrix} 0.0151 & 0 & 0.0144 \end{bmatrix} N.m.s \tag{25}$$

In order to bring out the presence of a singularity, the test was first performed with a Moore-Penrose allocation. Results are presented in Fig.4. Perturbations of large amplitude can be observed in angular momentum, due to the configuration staying for a long time in the vicinity of the singularity as shown by the determinant plot. Because of $\mathbf{Y}(\boldsymbol{\sigma})$ being poorly conditioned, the actuators are highly solicited with set-points exceeding the saturation value of 5 rad/s. Moore-Penrose trajectory is always orthogonal to the kernel space of $\mathbf{Y}(\boldsymbol{\sigma})$ since it locally minimizes $|| \dot{\boldsymbol{\sigma}} ||$.

Fig.5 shows the same direction followed with the EKF allocator. The presence of the singularity is indicated by the determinant being almost null between 4s and 6s. However, unlike the Moore-Penrose trajectory (Fig.4), the rotation speeds have non-null components in the kernel space between 4s and 6s, which allowed the cluster to reconfigure in order to escape the singularity. As a result, the rotation speeds are acceptable and stay far enough from saturation, even if they are higher than for the trajectory without singularity (Fig.3).

V. CONCLUSIONS

A general formulation of the EKF-based allocator was proposed, relying on the recent development of the contraction framework to maximize its convergence domain

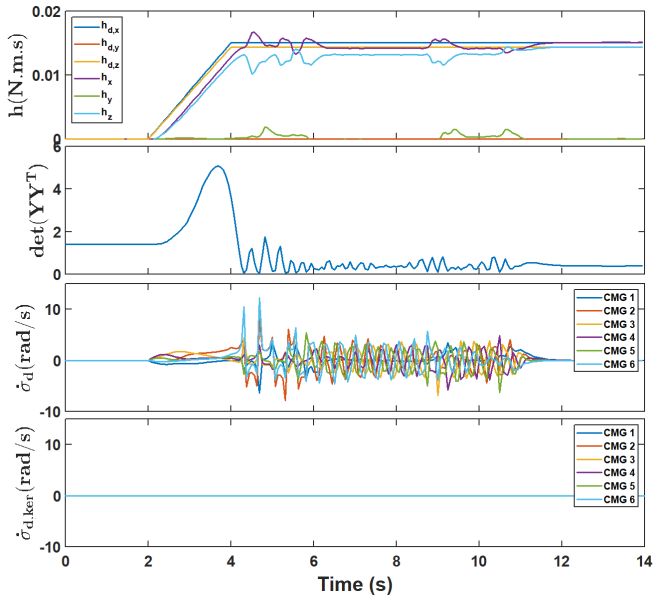

Fig. 4: Moore-Penrose allocation in presence of a singularity

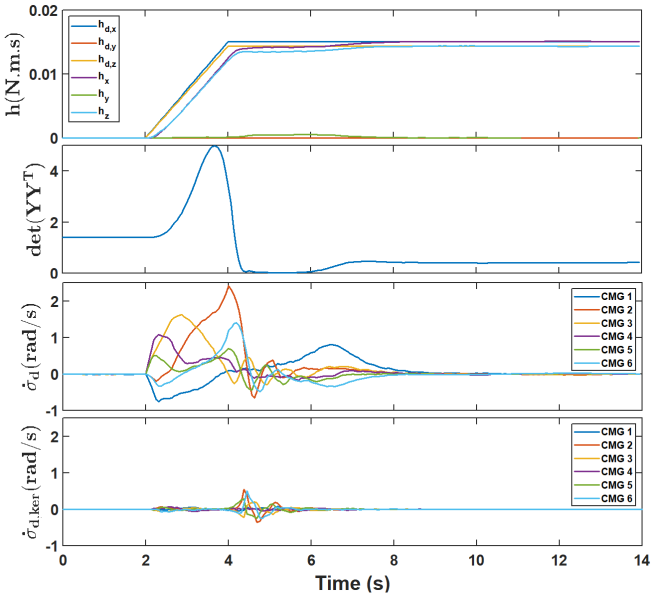

Fig. 5: Singularity avoidance with the EKF control allocation

with regard to the system specific parameters. While similar to optimization-based methods, the EKF-based allocator presents promising real-time capabilities, in particular for space applications where the computational cost is restricted. With this in mind, it was implemented on a test bench of Control Moment Gyros. Experimental tests showed that the actuators' efforts were minimized when no singularity was met, and that the singularity avoidance was performed by allowing small errors on the controlled output.

However, the singularity avoidance is purely reactive, based on balancing the increasing commands required by the loss of capacity in a singular direction. Theoretically, many of the singularities can be avoided without any error by re-configuring the actuators early enough in the trajectory. Future work will aim at including prior knowledge of the system configurations in order to anticipate the singularities before meeting them and thus ensuring avoidance without any error or delay on the controlled output.

ACKNOWLEDGMENT

This work is funded by ONERA, ISAE and CNES in the context of the COSOR project.

REFERENCES

[1] T. A. Johansen and T. I. Fossen, "Control allocation – a survey," *Automatica*, vol. 49, no. 5, pp. 1087–1103, 2013.

[2] H. Evain, M. Rognant, D. Alazard, and J. Mignot, "Nonlinear dynamic inversion for redundant systems using the ekf formalism," in *2016 American Control Conference (ACC)*. IEEE, 2016, pp. 348–353.

[3] B. Siciliano, "Kinematic control of redundant robot manipulators: A tutorial," *Journal of intelligent and robotic systems*, vol. 3, no. 3, pp. 201–212, 1990.

[4] C. W. Wampler, "Manipulator inverse kinematic solutions based on vector formulations and damped least-squares methods," *IEEE Transactions on Systems, Man, and Cybernetics*, vol. 16, no. 1, pp. 93–101, 1986.

[5] Y. Nakamura and H. Hanafusa, "Inverse kinematic solutions with singularity robustness for robot manipulator control," *Journal of dynamic systems, measurement, and control*, vol. 108, no. 3, pp. 163–171, 1986.

[6] B. Wie, "Singularity escape/avoidance steering logic for control moment gyro systems," *Journal of Guidance, Control, and Dynamics*, vol. 28, no. 5, pp. 948–956, 2005.

[7] S. R. Buss, "Introduction to inverse kinematics with jacobian transpose, pseudoinverse and damped least squares methods," *IEEE Journal of Robotics and Automation*, vol. 17, no. 1-19, p. 16, 2004.

[8] T. I. Fossen and T. A. Johansen, "A survey of control allocation methods for ships and underwater vehicles," in *2006 14th Mediterranean Conference on Control and Automation*. IEEE, 2006, pp. 1–6.

[9] M. Bodson, "Evaluation of optimization methods for control allocation," *Journal of Guidance, Control, and Dynamics*, vol. 25, no. 4, pp. 703–711, 2002.

[10] S. Bonnabel and J.-J. Slotine, "A contraction theory-based analysis of the stability of the extended kalman filter," *arXiv preprint arXiv:1211.6624*, 2012.

[11] L. Sciavicco and B. Siciliano, "A solution algorithm to the inverse kinematic problem for redundant manipulators," *IEEE Journal on Robotics and Automation*, vol. 4, no. 4, pp. 403–410, 1988.

[12] T. A. Johansen, "Optimizing nonlinear control allocation," in *2004 43rd IEEE Conference on Decision and Control (CDC)(IEEE Cat. No. 04CH37601)*, vol. 4. IEEE, 2004, pp. 3435–3440.

[13] J. Deyst and C. Price, "Conditions for asymptotic stability of the discrete minimum-variance linear estimator," *IEEE Transactions on Automatic Control*, vol. 13, no. 6, pp. 702–705, 1968.

[14] W. Lohmiller and J.-J. E. Slotine, "On contraction analysis for nonlinear systems," *Automatica*, vol. 34, no. 6, pp. 683–696, 1998.

[15] R. Olfati-Saber, "Kalman-consensus filter: Optimality, stability, and performance," in *Proceedings of the 48h IEEE Conference on Decision and Control (CDC) held jointly with 2009 28th Chinese Control Conference*. IEEE, 2009, pp. 7036–7042.

[16] H. W. Sorenson, "Least-squares estimation: from gauss to kalman," *IEEE spectrum*, vol. 7, no. 7, pp. 63–68, 1970.

[17] H. Evain, T. Solatges, A. Brunet, A. Dias Ribeiro, L. Sipile, M. Rognant, D. Alazard, and J. Mignot, "Design and control of a nano-control moment gyro cluster for experiments in a parabolic flight campaign," in *IFAC World Congress*, 2017.

[18] H. Evain, D. Alazard, M. Rognant, T. Solatges, A. Brunet, J. Mignot, N. Rodriguez, A. D. Ribeiro, *et al.*, "Satellite attitude control with a six-control moment gyro cluster tested under microgravity conditions," in *AIAC18: 18th Australian International Aerospace Congress (2019): ISSFD-27th International Symposium on Space Flight Dynamics (ISSFD)*. Engineers Australia, Royal Aeronautical Society., 2019, p. 1387.